Combination of cuprizone and experimental autoimmune encephalomyelitis to study inflammatory brain lesion formation and progression

Bernhard Josef Rüther, Miriam Scheld, Daniela Dreymueller, Tim Clarner, Eugenia Kress, Lars-Ove Brandenburg, Tine Swartenbroekx, Chloé Hoornaert, Peter Ponsaerts, Petra Fallier-Becker, Cordian Beyer, Sven Olaf Rohr, Christoph Schmitz, Uta Chrzanowski, Tanja Hochstrasser, Stella Nyamoya, Markus Kipp

Angaben zur Veröffentlichung / Publication details:

Rüther, Bernhard Josef, Miriam Scheld, Daniela Dreymueller, Tim Clarner, Eugenia Kress, Lars-Ove Brandenburg, Tine Swartenbroekx, et al. 2017. "Combination of cuprizone and experimental autoimmune encephalomyelitis to study inflammatory brain lesion formation and progression." *Glia* 65 (12): 1900–1913. https://doi.org/10.1002/glia.23202.

Combination of cuprizone and experimental autoimmune encephalomyelitis to study inflammatory brain lesion formation and progression

Bernhard Josef Rüther[1], Miriam Scheld[1], Daniela Dreymueller[2], Tim Clarner[1], Eugenia Kress[3], Lars-Ove Brandenburg[3], Tine Swartenbroekx[4], Chloé Hoornaert[4], Peter Ponsaerts[4], Petra Fallier-Becker[5], Cordian Beyer[1], Sven Olaf Rohr[6], Christoph Schmitz[6], Uta Chrzanowski[6], Tanja Hochstrasser[6], Stella Nyamoya[1,6], and Markus Kipp[6]

[1]Institute of Neuroanatomy and JARA-BRAIN, Faculty of Medicine, RWTH Aachen University, 52074 Aachen, Germany
[2]Institute of Pharmacology and Toxicology, Faculty of Medicine, RWTH Aachen University, 52074 Aachen, Germany
[3]Department of Anatomy and Cell Biology, RWTH Aachen University, 52074 Aachen, Germany
[4]Faculty of Medicine and Health Sciences, University of Antwerp, 2610 Antwerp, Belgium
[5]Institute of Pathology and Neuropathology, University of Tuebingen, 72076 Tuebingen, Germany
[6]Department of Anatomy II, Ludwig-Maximilians-University of Munich, 80336 Munich, Germany

Corresponding author:
Markus Kipp
Anatomische Anstalt; Lehrstuhl II - Neuroanatomie
Pettenkoferstr. 11; 80336 München
mail: markus.kipp@med.uni-muenchen.de

Funding information: Dr. Robert Pfleger Stiftung

Main points:

1. Cuprizone-induced cytodegeneration triggers monocyte, lymphocyte, and granulocyte recruitment into the forebrain.
2. Peripheral immune cell recruitment induces acute axonal injury.
3. Cytodegeneration augments cerebellar inflammation in experimental autoimmune encephalomyelitis.

Keywords: cuprizone, EAE, inflammation, multiple sclerosis

Abstract

Brain-intrinsic degenerative cascades are a proposed factor driving inflammatory lesion formation in multiple sclerosis (MS) patients. We recently described a model combining noninflammatory cytodegeneration (via cuprizone) with the classic active experimental autoimmune encephalomyelitis

(Cup/EAE model), which exhibits inflammatory forebrain lesions. Here, we describe the histopathological characteristics and progression of these Cup/EAE lesions. We show that inflammatory lesions develop at various topographical sites in the forebrain, including white matter tracts and cortical and subcortical grey matter areas. The lesions are characterized by focal demyelination, discontinuation of the perivascular glia limitans, focal axonal damage, and neutrophil granulocyte extravasation. Transgenic mice with enhanced green fluorescent protein-expressing microglia and red fluorescent protein-expressing monocytes reveal that both myeloid cell populations contribute to forebrain inflammatory infiltrates. EAE-triggered inflammatory cerebellar lesions were augmented in mice pre-intoxicated with cuprizone. Gene expression studies suggest roles of the chemokines *Cxcl10*, *Ccl2*, and *Ccl3* in inflammatory lesion formation. Finally, follow-up experiments in Cup/EAE mice with chronic disease revealed that forebrain, but not spinal cord, lesions undergo spontaneous reorganization and repair. This study underpins the significance of brain-intrinsic degenerative cascades for immune cell recruitment and, in consequence, MS lesion formation.

Introduction

Multiple sclerosis (MS) is a neuroinflammatory disorder of the central nervous system (CNS) with a high prevalence, especially in young adults. MS lesions are characterized by oligodendrocyte death, demyelination, gliosis, axonal damage, and peripheral immune cell infiltration (Bauer, Rauschka, & Lassmann, 2001; Benn, Halfpenny, & Scolding, 2001). MS is a clinically heterogeneous disorder that presents as a relapsing-remitting, secondary progressive, or primary progressive form (Lublin et al., 2014). Relapsing-remitting MS involves episodes or “attacks” of varied symptoms, including disturbances in vison and balance, dizziness, fatigue, incontinence, pain, muscle weakness or spasticity, and cognitive impairment. The frequency and severity of inflammatory attacks vary from patient to patient. In severe cases (i.e. Marburg's variant of MS), inflammatory demyelination can lead to severe functional deficits and sometimes dead (Nunes et al., 2015; Rush, MacLean, & Freedman, 2015). Some cases of MS are more benign, with no worsening of functional ability, even after 15 years of diagnosis, and low annualized relapse rates (Glad, Nyland, Aarseth, Riise, & Myhr, 2009; Sartori, Abdoli, & Freedman, 2017). However, in most cases, these attacks can recur with increasing frequency and proceed to secondary progressive MS, which, as with primary progressive forms, involves axonal damage and neurodegeneration (Charcot, 1868; Kornek et al., 2000; Trapp, Ransohoff, & Rudick, 1999) resulting in irreversible clinical disability. Despite decades of research, it is still not clear whether immune dysregulation or intrinsic cytodegenerative events are responsible for the formation of new lesions (Barnett & Prineas, 2004; Codarri, Greter, & Becher, 2013).

We recently demonstrated that primary oligodendrocyte degeneration can trigger peripheral immune cell recruitment into the forebrain (Scheld et al., 2016). In that study, oligodendrocyte apoptosis in the forebrains of mice was first induced by a 3-week treatment with cuprizone, and an infiltration of myelin autoreactive T cells from peripheral lymphoid organs was then triggered by experimental

autoimmune encephalomyelitis (EAE) via immunization with the myelin oligodendrocyte glycoprotein 35–55 peptide ($MOG_{35–55}$) (Iglesias, Bauer, Litzenburger, Schubart, & Linington, 2001). Our work and those of others (Baxi et al., 2015; Boretius et al., 2012) clearly illustrate the significance of brain-intrinsic degenerative cascades for immune cell recruitment and MS lesion formation.

The purpose of this study was to characterize the histopathology of inflammatory foci in our cuprizone-EAE model. Specifically, we sought to determine the composition of inflammatory infiltrates, which can include T lymphocytes and macrophages (Lucchinetti et al., 2000), as well as activated astrocytes and microglia and neutrophil granulocytes (Hertwig et al., 2016). We found that fluorescently labeled microglia and monocytes are both present in inflammatory lesions, with gene expression studies implicating the involvement of the chemokines C-X-C motif ligand 10 (CXCL10), C-C motif ligand 2 (CCL2), and C-C motif ligand 3 (CCL3) in inflammatory lesion formation. Finally, follow-up experiments revealed that, unlike spinal cord lesions, forebrain lesions exhibit spontaneous reorganization and repair.

Materials and Methods

Animals and experimental groups

C57BL/6 mice (Janvier Labs, Le Genest-Saint-Isle, France) were bred and maintained at a maximum of five animals per cage with *ad libitum* food and water in a pathogen-free environment. Cages were cleaned once per week and microbiological monitoring was performed according to the Federation of European Laboratory Animal Science Associations recommendations. Female 10-week-old (19–21 g) mice were randomly assigned to four groups (Fig. 1A): (i) control, animals received a diet of standard rodent chow for the duration of the 7-week study; (ii) cuprizone (Cup), animals were fed a diet containing 0.25% cuprizone [bis(cyclohexanone)oxaldihydrazone; Sigma-Aldrich Inc., St Louis, MO, USA] mixed into ground standard rodent chow for three weeks, followed by four weeks of normal chow; (iii) Cup/EAE, mice were fed the cuprizone diet for the first three weeks and were then immunized with $MOG_{35–55}$ at the beginning of week six; (iv) EAE, animals received the standard rodent chow for the duration of the study but were immunized with $MOG_{35–55}$ at the beginning of week six. An additional cohort of Cup/EAE animals was used to investigate inflammatory brain lesions during chronic disease, 47 days after immunization. A second study utilized female $CX_3CR1^{+/eGFP}/CCR2^{+/RFP}$ reporter gene transgenic mice [C57BL/6 background; (Dooley et al., 2016; Le Blon et al., 2016)] with green fluorescent microglia and red fluorescent infiltrating macrophages/monocytes under the same experimental conditions to discriminate brain-resident microglia from infiltrating peripheral monocytes/macrophages.

EAE and disease scoring

To induce the formation of myelin autoreactive T cells, mice were immunized with an injection of an emulsion of $MOG_{35–55}$ peptide dissolved in complete Freund's adjuvant followed by injections of

pertussis toxin in PBS on the day of and the day after immunization (Hooke Laboratories, USA). Disease severity was scored as follows: 1, the entire tail drapes over the observer's finger when the mouse is picked up by base of the tail; 2, the legs are not spread apart but held close together when the mouse is picked up by base of the tail, and mice exhibit a clearly apparent wobbly gait; 3, the tail is limp and mice show complete paralysis of hind legs (a score of 3.5 is given if the mouse is unable to raise itself when placed on its side); 4, the tail is limp and mice show complete hind leg and partial front leg paralysis, and the mouse is minimally moving around the cage but appears alert and feeding (a score of 4 was not attained by any of the mice in our study).

Tissue preparation

For histological and immunohistochemical studies, mice were anaesthetized with ketamine (100 $mg \cdot kg^{-1}$ i.p.) and xylazine (10 $mg \cdot kg^{-1}$ i.p.) and transcardially perfused with ice-cold PBS followed by a 3.7% paraformaldehyde solution (PFA; pH 7.4). Brains were postfixed overnight in PFA, dissected, embedded in paraffin, and then coronal sections (5 µm) were cut (Acs et al., 2009; Clarner et al., 2012). Spinal cords were incubated in EDTA (ethylenediaminetetraacetic acid) solutions for 48 h (changed once) at 37°C prior to paraffin embedding. This decalcification procedure was not performed for samples from some EAE mice to enable the enzymatic detection of neutrophils. For gene expression studies, tissues were manually dissected after transcardial PBS perfusion, immediately frozen in liquid nitrogen, and kept at -80°C until further processing. For ultrastructural analyses by electron microscopy, tissue preparation was performed according to protocols published previously by our laboratory (Norkute et al., 2009).

Immunohistochemistry and neutrophil staining

For immunohistochemistry, sections were rehydrated and, if necessary, antigens were unmasked with Tris/EDTA buffer (pH 9.0) or citrate (pH 6.0) heating. After washing in PBS, sections were incubated overnight (4°C) with the following primary antibodies diluted in blocking solution (serum of species in which the secondary antibody was produced). Anti-glial fibrillary acidic protein antibody ([GFAP] 1:12,000; EnCor Biotechnologie Inc, Gainesville, FL, USA) was used to visualize astrocytes, anti-ionized calcium-binding adaptor molecule 1 antibody ([Iba1] 1:10,000; Wako Chemicals GmbH, Neuss, Germany) was used to detect microglia/macrophages, and anti-amyloid precursor protein antibody ([APP] 1:5,000, Merck-Millipore) was used to detect acute axonal damage (Bitsch, Schuchardt, Bunkowski, Kuhlmann, & Bruck, 2000; Gehrmann, Banati, Cuzner, Kreutzberg, & Newcombe, 1995; Kuhlmann, Lingfeld, Bitsch, Schuchardt, & Bruck, 2002; Pfeifenbring et al., 2015; Schirmer, Merkler, Konig, Bruck, & Stadelmann, 2013). The next day, slides were incubated with biotinylated secondary antibodies for 1 h and then with peroxidase-coupled avidin-biotin complex (ABC kit; Vector Laboratories, Peterborough, UK) and treated with 3,3′-diaminobenzidine (DAKO, Hamburg, Germany) as a peroxidase substrate or incubated with Alexa Fluor-coupled secondary antibodies (Life

Technologies, Germany) as published previously (Hoflich et al., 2016). Luxol fast blue (LFB)/periodic acid-Schiff stains were performed following established protocols. To visualize granulocytes in paraffin-embedded tissues, a naphthol AS-D chloroacetate (specific esterase) kit was used (Sigma-Aldrich, Germany).

Stained and processed sections were digitalized using a Nikon ECLIPSE E200 microscope (Nikon, Nikon Instruments, Düsseldorf, Germany) equipped with a DS-Vi1 camera. To analyze microglia/monocyte densities in the cerebelli, Iba1 immunoreactivity was scored as ranging from 1 (baseline "normal" reactivity) to 5 (maximum reactivity) by two evaluators blinded to the treatment groups, and the results were averaged. The open source program ImageJ (NIH, Bethesda, MD, USA) was used to determine cellular densities and to quantify the numbers of APP^+ spheroids at specified distances from inflamed vessels. To quantify the numbers and localization of perivascular infiltrates in the forebrain and cerebellum, lesions were identified in hematoxylin and eosin (H&E)-stained sections by two evaluators blinded to the treatment groups, and the results were averaged. Forebrains were analyzed at the levels R235 and R275 according to the mouse brain atlas by Sidman et al. (http://www.hms.harvard.edu/research/brain/atlas.html), whereas cerebelli were analyzed at the levels R465 and R485.

Discrimination of microglia and recruited monocytes in $CX_3CR1^{+/eGFP}/CCR2^{+/RFP}$ mice

All immunofluorescence analyses were performed according to previously described procedures (Dooley et al., 2016; Le Blon et al., 2016). Briefly, mice were transcardially perfused with a 0.9% NaCl solution followed by 4.0% PFA. Next, brains were isolated, further fixed in 4.0% PFA for 3 h, and then protected through a gradient of 5%, 10%, and 20% sucrose. Afterwards, brain tissue was snap-frozen in liquid nitrogen and kept at -80°C until further processing. Cryosections (10 µm) were cut using an HM500 cryostat and incubated first with a rabbit anti-RFP antibody (2.5 µg/mL, ab62341; Abcam) and then a secondary donkey anti-rabbit Alexa Fluor 555 antibody (2 µg/mL, A31572; Invitrogen). Nuclear staining was performed using TO-PRO-3 (1:200; Life Technologies) and sections were mounted with Prolong Gold anti-fading reagent. Images were acquired using a BX51 fluorescence microscope equipped with an Olympus DP71 digital camera and processed with Olympus cellSens dimension software. Quantitative analysis of $eGFP^+$ brain-resident microglia and infiltrating RFP^+ peripheral monocytes/macrophages was performed using the TissueQuest immunofluorescence analysis software (v3.0; TissueGnostics GmbH). After manually delineating the region of interest (midline of the corpus callosum) using ImageJ, the total numbers of TO-PRO-3^+ nuclei and those colocalizing with a direct eGFP fluorescence signal and/or antibody-stained anti-RFP fluorescence signal were automatically determined using TissueQuest software. Each staining/analysis was performed in duplicate.

Transmission electron microscopy

Tissue samples were fixed with 2.5% glutaraldehyde (Science Services, Munich, Germany) in cacodylate buffer (pH 7.4; Merck-Millipore, Darmstadt, Germany) at 4°C overnight as described previously (Noell et al., 2012). Thereafter, samples were embedded in Araldite (Serva, Heidelberg, Germany), and ultrathin sections were cut using a Leica ultramicrotome (Leica, Wetzlar, Germany) and analyzed using a Zeiss EM-10 transmission electron microscope (Zeiss, Oberkochen, Germany).

Gene expression analyses

Gene expression levels were measured by real-time reverse transcription-PCR ([qRT-PCR] Bio-Rad, Munich, Germany) using SensiMix Plus SYBR and fluorescein (Quantace, Bioline, Luckenwalde, Germany) with a standardized protocol as described previously by our group (Slowik et al., 2015). Primer sequences and individual annealing temperatures are shown in Table 1. Relative quantification was performed using the ΔΔCt method with β actin as the reference gene. Melting curves and gel electrophoresis of the PCR products were routinely performed to determine the specificity of the PCR reactions (data not shown).

Flow cytometry analysis of primary blood cells

Peripheral blood samples (400 µL, citrated 0.38%) were subjected to erythrocyte lysis (155 mM NH_4Cl, 10 mM $NaHCO_3$, 5 mM EDTA, pH 7.4) and resuspended in assay buffer (PBS with 1% fetal bovine serum and 1 mM EDTA); all steps of the staining process were performed at 4°C. Prior to staining for forkhead box P3 (FOXP3) and interferon γ, cells were first permeabilized with 0.1% Triton-X 100 in PBS. For cell surface staining the differentiation of T-helper cell subsets, blood samples were stained with anti-CD4-allophycocyanin-H7, anti-CD25-allophycocyanin, anti-IL17A, and FOXP3-fluorescein (BD Pharmingen), and anti-interferon γ-PB (eBioscience). For the differentiation of leukocyte subsets, samples were stained with anti-Ly6G-allophycocyanin (Miltenyi Biotec), anti-F4/80-phycoerythrin (Serotec), anti-CD4-allophycocyanin-H7, and anti-CD8-PB (BD Pharmingen). Samples were analyzed using a FACS LSR Fortessa (BD Biosciences) with FlowJo software.

Statistical analysis

Statistical analyses were performed using Prism 5 (GraphPad Software Inc., San Diego, CA, USA). All data are given as arithmetic means ± SEMs. A p value of <0.05 was considered to be statistically significant.

Results

Clinical progression of symptoms in Cup/EAE and EAE mice

As expected, control and cuprizone-intoxicated mice did not show any clinical signs of disease. However, EAE and Cup/EAE mice exhibited signs of disease progression beginning ~11 days after

immunization (10.8 ± 0.58 vs. 11.0 ± 0.31 days; $p = 0.77$) (Fig. 1B). There was no difference between these groups in the average maximum disease score (2.3 ± 0.34 vs. 2.8 ± 0.25; $p = 0.27$). In line with these observations, the histopathological appearance of spinal cord tissues (Fig. 1C) and the numbers of spinal inflammatory infiltrates (Fig. 1D) were comparable in Cup/EAE and EAE animals. Such lesions were present at several topographical sites, including the ventral, lateral, and dorsal funiculi, with all segments (i.e., cervical, thoracic, lumbar, and sacral) of the spinal cord affected equally.

Distribution of inflammatory forebrain lesions

As previously described (Scheld et al., 2016), focal inflammatory infiltrates in our model are characterized by perivascular immune cell accumulation (i.e., within an enlarged Virchow-Robin space), perivascular astrocytosis, and demyelination (see Fig. 2A). Recruited inflammatory cells frequently progressed through the astrocytic glia limitans perivascularis to invade the surrounding neuropil. GFAP immunoreactivity was increased around the lesions, and focal demyelination was pronounced in lesions where peripheral immune cells had invaded the perivascular neuropil. H&E stains were performed to visualize the number and distributions of these lesions in brain sections at two levels of the forebrain from animals sacrificed at the peak of the disease (i.e., at day 14 postimmunization) (Fig. 2B). Loci of perivascular infiltrates were absent in the brains of control and cuprizone-intoxicated animals, and there were few in EAE-immunized animals that were primarily periventricular. By contrast, many loci of perivascular infiltrates were present in Cup/EAE animals, and these lesions were widely distributed throughout the corpus callosum and cortical and subcortical grey matter areas.

To test for the presence of acute axonal injury around inflammatory infiltrates, lesions were identified in H&E-stained slides and adjacent sections were stained for APP, a well-known marker for acute axonal injury (Hoflich et al., 2016). Under pathological conditions, anterograde axonal transport is disturbed and APP accumulates as ovoid spheroids (Kuhlmann et al., 2002). Therefore, we measured the densities of APP^+ spheroids in concentric areas around the vessel centers. As shown in Fig. 2C, spheroid densities were highest in the immediate vicinity of the inflamed vessel and progressively declined with increasing distance. This result lead us to conclude that inflammatory infiltrating peripheral immune cells, either lymphocytes or monocytes, focally induce acute axonal injury.

Characterization of inflammatory response

The composition of peripheral inflammatory cells was determined via flow cytometry analysis of blood samples collected during the peak phase of the disease (i.e., directly before the animals were sacrificed). EAE and Cup/EAE mice had higher numbers of total leucocytes (Fig. 3A), neutrophils (Fig. 3B), $CD4^+$ lymphocytes (Fig. 3C), and monocytes ($F4/80^+$ cells; Fig. 3D) than controls and Cup mice. For a more fine-grained analysis, we further quantified the total numbers of $CD4^+CD25^+FOXP3^+$ regulatory T cells and $CD4^+Th17^+$ effector T cells in peripheral blood. In line with reported findings (Korn et al., 2007; McGeachy, Stephens, & Anderton, 2005), the numbers of regulatory T cells were comparable in control,

cuprizone, and EAE mice, whereas a significant induction was observed in Cup/EAE mice (Fig. 3E). Whereas the numbers of Th17 effector T cells were slightly increased in Cup and EAE mice, there was a significant induction in Cup/EAE mice (Fig. 3F). As flow cytometry revealed a higher number of neutrophils in Cup/EAE animals, and other studies in EAE indicate that neutrophils have an important role in inflammation (Y. Liu et al., 2015; Pierson, Wagner, & Goverman, 2016), we examined ultrastructural as well as enzymatically stained images to identify neutrophils in perivascular infiltrates (Fig. 3G). Using both techniques, high numbers of neutrophils were found in the perivascular compartment and in the forebrain parenchyma, with densities of ranging from 1,778 to 12,526 cells/mm^2 (mean, 4,614 ± 359 granulocytes/mm^2) in the proximity of perivascular forebrain lesions. As shown in Fig. 3G (lower right), the density of neutrophil granulocytes in perivascular forebrain lesions of Cup/EAE mice was comparable to that found in the spinal cords of EAE mice (4,614 ± 359 cells/mm^2 vs. 3,647 ± 357.5 granulocytes/mm^2; $p = 0.083$).

Microglia activation and Monocyte recruitment in Cup/EAE animals

The activation of microglia and recruitment of monocytes in sites of demyelination that are characteristic of MS lesions are not observed in the cuprizone mouse model (McMahon, Suzuki, & Matsushima, 2002). To determine if these occur in our Cup/EAE model, we utilized transgenic ($CX_3CR1^{+/eGFP}/CCR2^{+/RFP}$) mice with eGFP-expressing microglia and RFP-expressing monocyte-derived macrophages (Saederup et al., 2010). The numbers of forebrain eGFP$^+$ microglia were within the physiological range in control and EAE mice but significantly increased in Cup and Cup/EAE mice (Fig. 4A,B). By contrast, numbers of RFP$^+$ monocyte-derived macrophages were only significantly elevated in Cup/EAE mice. These results clearly demonstrate that, whereas forebrain microglial activation is not characteristic of the EAE model, significantly more microglia as well as monocytes are recruited to the forebrain lesions of Cup/EAE mice.

Peripheral immune cell recruitment is paralleled by the induction of adhesion molecules

We next analyzed the expression of genes encoding cell adhesion molecules in the corpus callosa of experimental mice. To validate this method, we compared the quantification of GFAP$^+$ reactive astrocytes by immunohistochemistry with transcript levels by qRT-PCR. Both methods revealed similar significant increases in GFAP in Cup and Cup/EAE animals compared with control mice (Fig. 5A). Therefore, we measured the transcript levels of intercellular adhesion molecule 1 (*Icam1*) and vascular cell adhesion molecule 1 (*Vcam1*) in our experimental groups. Strikingly, both were significantly increased only in Cup/EAE mice (Fig. 5B).

Cuprizone intoxication augments cerebellar immune cell infiltration

In the forebrain, the interplay between innate immune activation (via cuprizone intoxication) and adaptive immunity (via EAE) is used to model MS disease activity. As both models also impact the

cerebellum (Groebe et al., 2009; Skripuletz et al., 2010), we investigated this region to determine whether changes are augmented in our Cup/EAE model. Similar to what we observed in the forebrain, there were many loci of perivascular infiltrates in the cerebella of Cup/EAE mice, and virtually none in control and Cup mice, as well as in cuprizone-treated mice "immunized" with complete Freund's adjuvant and pertussis toxin only (lacking the $MOG_{35–55}$ peptide) (Fig. 6A). Although a moderate number of loci were present in EAE mice, significantly more were detected in Cup/EAE mice (10 ± 2.1 vs. 32 ± 4.3 loci per slide; $p = 0.008$), and could be found in the cerebellar cortex, arbor vitae and deep cerebellar white matter, and in the adjacent brainstem. To determine if this peripheral immune cell recruitment in the cerebellum is paralleled by an increase in microglia/monocyte activity, we performed immunohistochemistry for the microglia/monocyte pan-marker Iba1, and staining intensity was quantified by visual scoring (1–5; see Fig. 6C,D). The cerebella of Cup and EAE mice showed an expected increase in microglia/monocyte reactivity, whereas the increase was significantly higher in Cup/EAE mice.

Increased chemokine expression in Cup/EAE mice.

As chemokines have a central role in orchestrating innate and adaptive immune responses (Hartung, Aktas, Menge, & Kieseier, 2014), we assessed the expression of *Cxcl10*, *Ccl2*, and *Ccl3* in the corpus callosa, cerebella, and spinal cords of experimental mice. *Cxcl10* levels were significantly increased in the cerebella and spinal cords of EAE mice, and were significantly higher in all three areas in Cup/EAE mice (Fig. 7A). A similar expression pattern was observed for *Ccl2* (Fig. 7B). Of note, expression patterns for *Ccl3* differed among the regions. In the spinal cord, the pattern of *Ccl3* expression was similar to those of *Cxcl10* and *Ccl2*, with a significant increase over controls in the EAE group and even higher expression in Cup/EAE mice. However, in the corpus callosum and cerebellum, *Ccl3* expression was significantly induced in Cup and Cup/EAE mice; no induction was observed in EAE mice. These results demonstrate a region- and chemokine-specific induction of inflammatory cytokines.

Repair of inflammatory forebrain lesions

To examine the progression of inflammatory forebrain lesions in Cup/EAE mice, we sacrificed a cohort of animals approximately 7 weeks after $MOG_{35–55}$ immunization (i.e., the chronic group) (Fig. 8A). After the peak of clinical disease, clinical scores in Cup/EAE animals abated somewhat but the animals remained clinically impaired until the end of the observation period (Fig. 8B). To verify that these clinical scores reflect the extent of inflammation in the spinal cord, we examined the histopathology of the spinal cords. In line with our behavioral observations, inflammatory demyelination within the spinal cord white matter of Cup/EAE animals was still present during the chronic stage. In LFB/periodic acid-Schiff stained sections, ~5.3% of the entire white matter was affected in chronic Cup/EAE groups, comparable to the 4.4% affected in Cup/EAE mice at the peak of clinical disease (~2 weeks after immunization in the "acute" group). However, chronic lesions were less inflammatory than acute

lesions, but showed marked loss of LFB staining (Fig. 8C). This difference in LFB staining intensity was not due to differences in tissue processing during the staining procedure. Thus, the spinal cord pathology remained stable during chronic disease. Next, we investigated the forebrains at distinct rostral to caudal levels for the presence of inflammatory infiltrates during chronic disease. To our great surprise, there were substantially fewer inflammatory infiltrate foci in forebrains of animals sacrificed during the chronic stage than in those sacrificed at the acute stage (Fig. 8D). The majority of lesions were found around the third ventricle and within the striatum.

Discussion

We recently developed a novel MS animal model characterized by multifocal inflammatory forebrain lesions (Scheld et al., 2016). In this study, we characterized these lesions at the cellular level and found that they are dominated by microglia and infiltrating monocytes. Specifically, our results show (i) that in the cuprizone model, peripheral monocyte recruitment is not a dominant feature, (ii) that the corpus callosum is not a predilection site in $MOG_{35–55}$-induced EAE, and (iii) that brain-intrinsic degenerative processes induced by cuprizone support the opening of the blood-brain-barrier (BBB) and facilitate the recruitment of peripheral monocytes to the lesion sites (Alvarez, Katayama, & Prat, 2013).

The integrity of the BBB and the contribution of peripheral immune cells to cuprizone-induced pathology is controversial in the literature. After cuprizone-induced acute demyelination, no BBB disruption has been detected by horseradish peroxidase tracing or immunohistochemical staining for serum proteins, despite robust microglial and astrocytic responses (Bakker & Ludwin, 1987; Kondo, Nakano, & Suzuki, 1987). Moreover, gadolinium magnetic resonance imaging in mice did not reveal a disturbance of BBB integrity after 5 weeks of cuprizone intoxication (Boretius et al., 2012). Histologically, these lesions did not exhibit deposition of immunoglobulins or fibrinogen, markers of lost BBB integrity. In contrast to these data, a recent report demonstrated extravasation of Evans blue dye into the CNS of cuprizone-fed mice, indicating minor loss of BBB integrity (Berghoff et al., 2017). In addition, a study by McMahon and colleagues (McMahon et al., 2002) showed that a small number of peripheral macrophages do indeed migrate into the brain in response to cuprizone-induced demyelination. However, their study involved brain irradiation to generate the GFP bone marrow chimeric mice, a treatment that was suggested to be responsible for the observed effect (Mildner et al., 2007). Furthermore, recombinase activating gene 1 (RAG1)-deficient mice that lack T and B cells are fully vulnerable to cuprizone-induced demyelination, indicating that T and B cells are not required or involved in this model (Hiremath, Chen, Suzuki, Ting, & Matsushima, 2008). Nevertheless, early and transient recruitment of C-X-C motif chemokine receptor 2-expressing neutrophils has been implicated in cuprizone-induced demyelination (L. Liu et al., 2010). Overall, the results from most studies suggest that peripheral immune cells have negligible significance in cuprizone-induced pathology, which instead is characterized by microglia accumulation. Consistent with this, we observed a significant increase in microglia in Cup mice.

Inflammatory lesions in $MOG_{35–55}$-induced EAE are primarily observed in the spinal cord, cerebellum, and optic nerve (Kuerten et al., 2007; Scheld et al., 2016). Our data show that cuprizone intoxication permits involvement of the forebrain in EAE. We hypothesize that this occurs via a three-step process. First, cuprizone activates cells of the BBB (i.e. astrocytes, pericytes, and endothelial cells), compromising its integrity. Second, encephalitogenic immune cells invade the forebrain parenchyma and are locally reactivated. Third, a secondary wave of immune cell recruitment results in the inflammatory demyelinating lesions. Thus, there must be identifiable factors in Cup/EAE mice that contribute to these steps.

We found that the expression of specific cell adhesion molecules was induced exclusively in Cup/EAE mice, suggesting that these treatments have produced an environment conducive to inflammatory cell activity. Moreover, we identified upregulation of *Ccl2*, *Ccl3*, and *Cxcl10*, which encode chemokines that act as chemoattractants for various inflammatory cells, including T lymphocytes (Carr, Roth, Luther, Rose, & Springer, 1994; K. K. Liu & Dorovini-Zis, 2012; Millward, Caruso, Campbell, Gauldie, & Owens, 2007), dendritic cells (Xu, Warren, Rose, Gong, & Wang, 1996), monocytes (Moreno et al., 2014; Price et al., 2014), and microglia (Clarner et al., 2015; Moreno et al., 2014). Interestingly, the cerebella of mice showed relatively weaker induction of these chemokines, despite that obvious involvement of this region in EAE by our work and those of others. For instance, the induction of *Ccl3* expression is moderate in the cerebella of EAE-diseased mice. Thus, it is possible that distinct chemokines regulate peripheral immune cell recruitment in particular brain regions. A clearer understanding of this is of vital importance for developing future therapeutic anti-chemokine strategies. If, for example, CCL3 regulates inflammation in the brain but not in the cerebellum, patients with greater forebrain involvement would benefit from anti-chemokine strategies that target CCL3.

Myeloid cells predominate in active MS brain lesions (Lucchinetti et al., 2000; Werner, Bitsch, Bunkowski, Hemmerlein, & Bruck, 2002), and recently, the neutrophils have increasingly become the focus of EAE studies where they migrate from the blood into the spinal cord parenchyma early during the disease course (Aube et al., 2014; Wu, Cao, Yang, & Liu, 2010). Indeed, the recruitment of neutrophils is an early and transient event (Aube et al., 2014; Wu et al., 2010), and depletion delays the clinical manifestation of EAE and prevents disruption of the blood-spinal cord-barrier (Aube et al., 2014; Steinbach, Piedavent, Bauer, Neumann, & Friese, 2013). In addition, the blockade of the neutrophil-specific chemokine receptor CXCR2 renders mice resistant to EAE (Carlson, Kroenke, Rao, Lane, & Segal, 2008). Our results show that neutrophil granulocytes were among the recruited immune cells, for which the stimulation of has been shown to promote EAE (Kilic et al., 2015). Thus, it is believed that granulocytes are important contributors in preparing for CNS inflammation by priming microglia and inducing their maturation (Steinbach et al., 2013). Whereas we observed low granulocyte numbers in the peripheral blood of control and cuprizone-treated animals, high numbers were observed in the blood of EAE and Cup/EAE mice as well as in the forebrains of Cup/EAE mice. Nevertheless, the relevance of these cells for inflammatory forebrain lesion development in Cup/EAE mice remains to be clarified.

One important question is which factor(s) triggers granulocyte recruitment into the forebrain. It is well known that the development of Th17 cells is a key event in the pathogenesis of $MOG_{35–55}$-induced EAE (Cua et al., 2003; Park et al., 2005; Serada et al., 2008), and adoptively transferred $CD4^+$ T cells secreting IL-17, the signature Th17 cytokine, migrate into the corpus callosa of cuprizone-fed mice (Baxi et al., 2015). IL-17 induces neutrophil-mobilizing/activating factors, including chemokines that target granulocytes, such as CXCL1, CXCL2, and CXCL5 (Iwakura, Ishigame, Saijo, & Nakae, 2011). Brain-intrinsic synthesis of IL-17 has been shown to promote granulocyte infiltration and aggravate myelin loss and behavioral deficits in the cuprizone model (Zimmermann et al., 2017). This suggests that Th17 lymphocytes infiltrate the forebrain in our Cup/EAE model and recruit granulocytes. Along this line, neutrophils that infiltrate the CNS may secrete soluble factors—most likely several proinflammatory proteins—that contribute to the maturation of antigen-presenting cells and affect the reactivation of myelin antigen-specific T cells. Indeed, it was shown that bone marrow-derived dendritic cells exposed to neutrophils from EAE spinal cord express MHC class II and the costimulatory molecules CD80 and CD86 (Steinbach et al., 2013), thus potentially increasing their capacity to restimulate effector T cells. Further studies are needed to determine whether recruited granulocytes in the Cup/EAE model are able to activate microglia and enhance their capacity to restimulate effector T cells in a similar manner.

A final important observation from this study was that the forebrain lesions in Cup/EAE mice are self-limiting (i.e. show spontaneous resolution), whereas lesions located in the spinal cord are not. The reason for this discrepancy is currently unclear. However, a detailed comparison of spinal cord and forebrain lesions at the molecular and cellular levels will help to elucidate the factors potentially involved in inflammatory lesion progression and/or resolution.

In summary, our findings add to our understanding of the Cup/EAE model, a practical and effective tool for studying immune cell recruitment in MS. Of note, the model has great translational potential, as most imaging and pathological MS studies are performed in the forebrain. By contrast, most EAE studies focus on spinal cord lesions. The presented Cup/EAE model will provide valuable insight into inflammatory lesion development and progression in the forebrain.

Acknowledgements

This study was supported by the Dr. Robert Pfleger Stiftung (M.K.). The technical support from P. Ibold, H. Helten, S. Wübbel, B. Aschauer, and A. Baltruschat is acknowledged.

Conflict of interest:

The authors declare no competing financial interests.

Figures

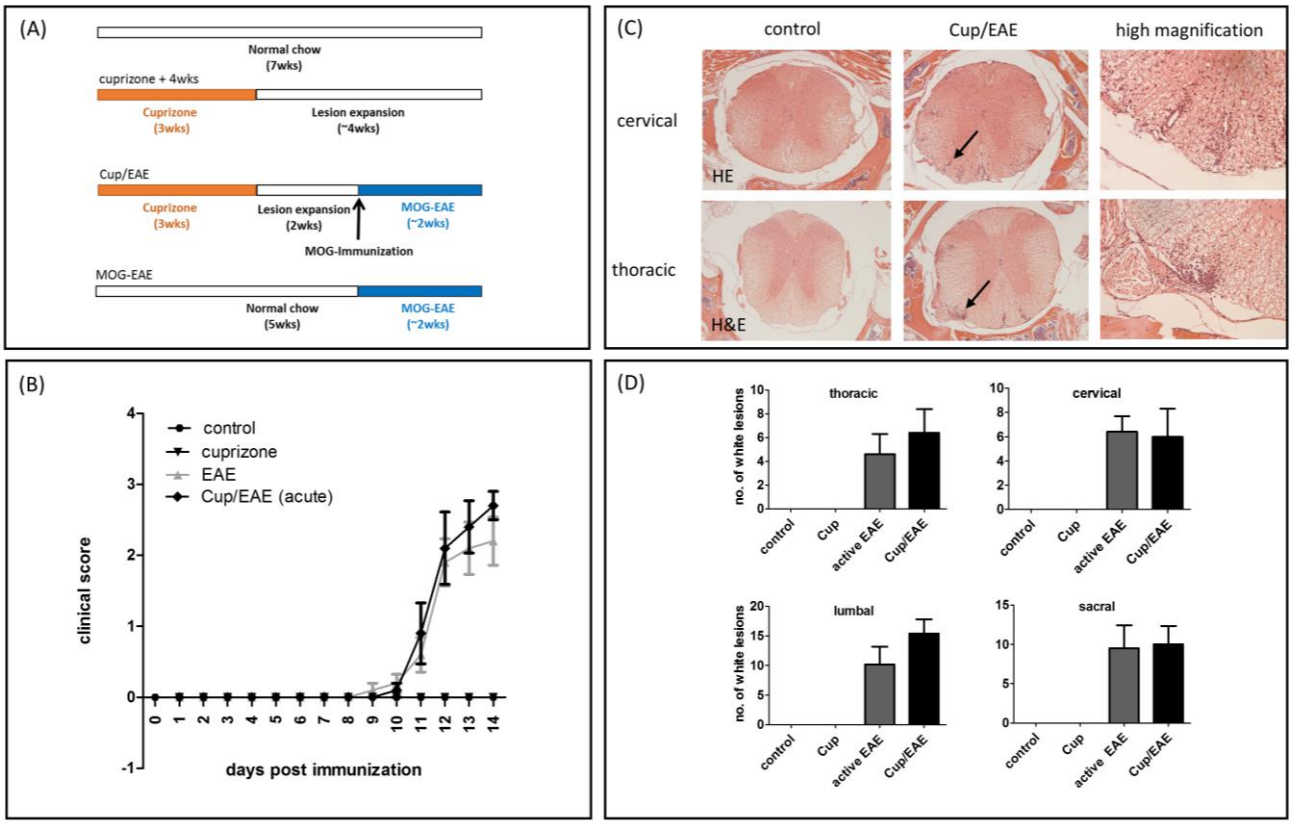

Figure 1. Clinical disease progression.

(A) Schematic depicting the experimental setup. Periods of cuprizone intoxication are highlighted in orange, whereas periods of $MOG_{35–55}$ immunization and subsequent active EAE development are highlighted in blue. (B) Clinical scores for control, EAE, and Cup/EAE mice. (C) Representative H&E-stained spinal cord sections from control and Cup/EAE mice. Images at higher magnification are regions indicated by arrows in Cup/EAE images. (D) Quantification of inflammatory infiltrates in spinal cords at different levels.

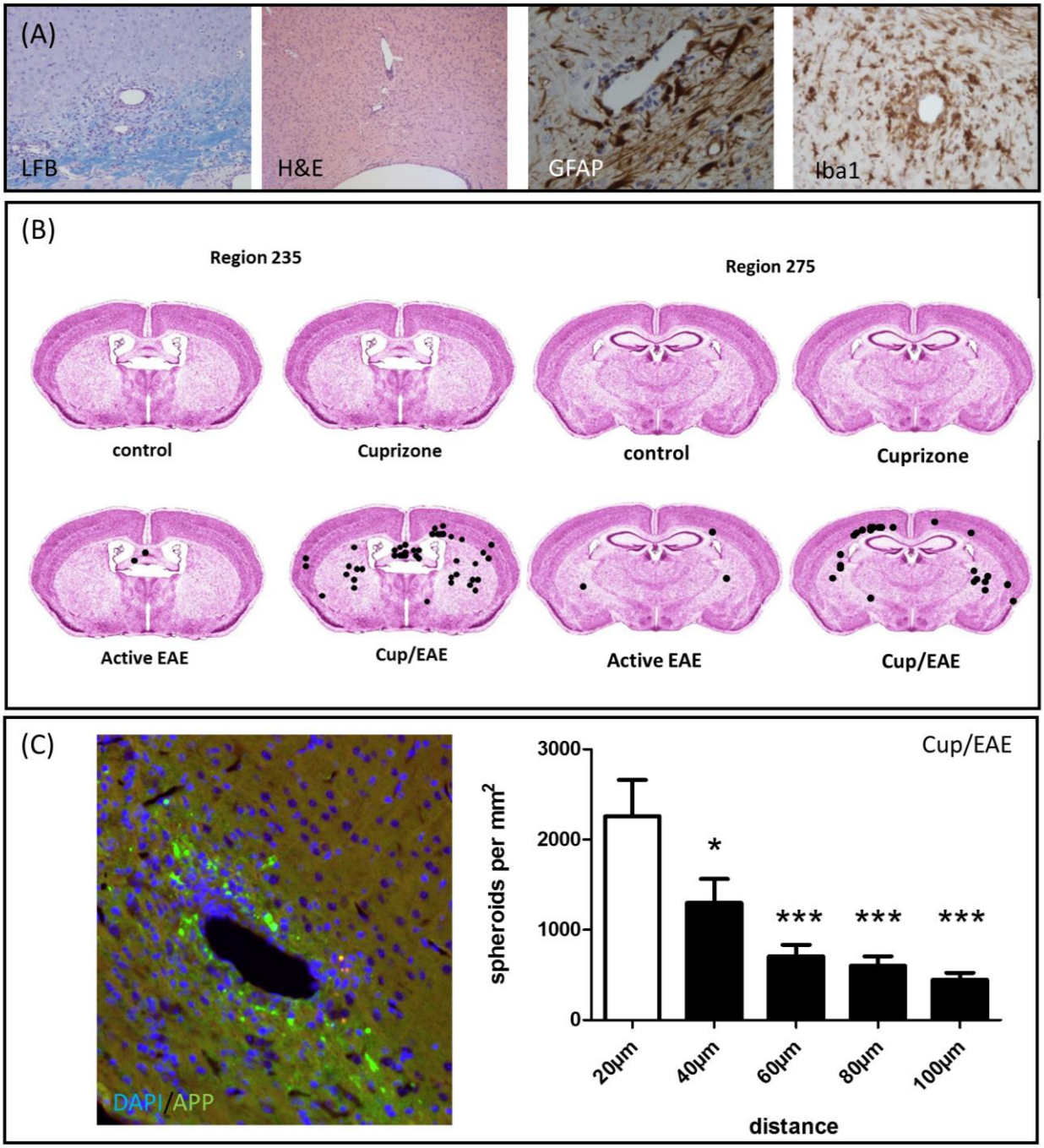

Figure 2. Forebrain inflammatory cell infiltration.

(A) Histopathological characteristics of inflammatory forebrain lesions in Cup/EAE mice. Immune cell neuropil invasion induces focal demyelination (shown with LFB), which is paralleled by the breakdown of the glia limitans perivascularis (shown with GFAP immunoreactivity) and accumulation of microglia/monocytes (shown with Iba1 immunoreactivity). (B) Distribution of perivascular infiltrates in the different treatment groups (H&E staining; black dots from one independent observer) at two brain levels (regions according to Sidman et al.). (C) Perivascular acute axonal injury visualized by anti-APP immunohistochemistry. APP^+ spheroid density was determined in concentric areas (up to 100 µm) from the vessel center. Differences determined using one-way ANOVA with Dunnett's post-hoc test; *p < 0.05 and ***p < 0.001 vs. 20 µm.

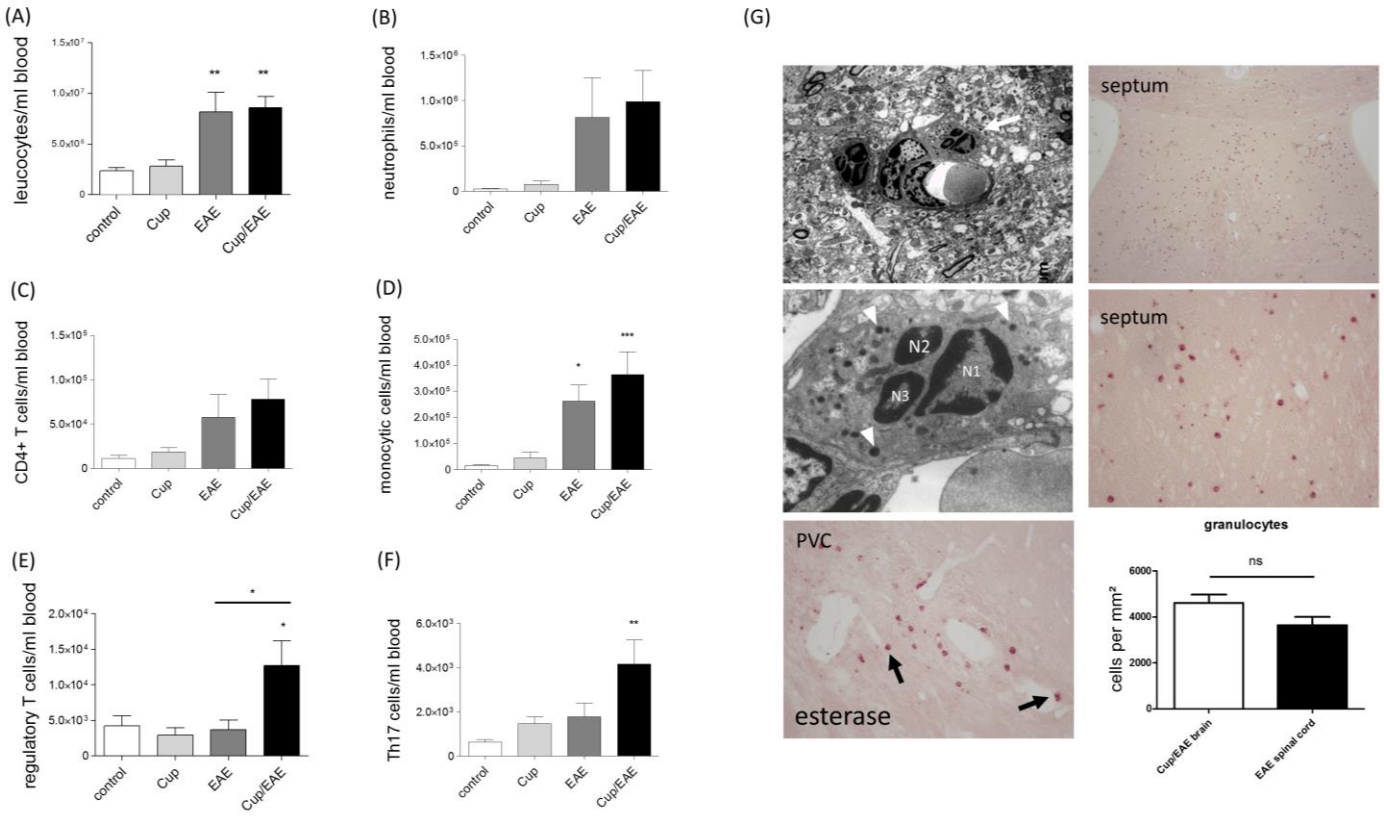

Figure 3. Peripheral inflammatory response.

(A–F) Absolute cell numbers were determined in peripheral blood samples of control, Cup, EAE, and Cup/EAE mice. Numbers of total leucocytes (determined via CountBright Beads; Molecular Probes) (A), neutrophil granulocytes ($Ly6G^+F4/80^-$) (B), Th lymphocytes ($CD4^+$) (C), monocytes ($F4/80^+$) (D), regulatory T lymphocytes ($CD4^+CD25^+FOXP3^+$) (E), and Th17 lymphocytes ($CD4^+IL17^+$) (F). Differences between groups determined using one-way ANOVAs with Dunnett's post-hoc tests; $*p < 0.05$, $**p < 0.01$, and $***p < 0.001$ vs. control. (G) Ultrastructural imaging (upper, middle left) of infiltrating neutrophils. Note the segmented nucleus (N1–N3) as well as numerous lysosomes (arrowheads). Naphthol AS-D chloroacetate (esterase) staining (bottom left) revealed granulocytes (pink cells; arrows) around vessels and within the neuropil. (bottom right) Similar densities of neutrophils were detected in inflammatory forebrain infiltrates of Cup/EAE mice and in spinal cord infiltrates in EAE mice.

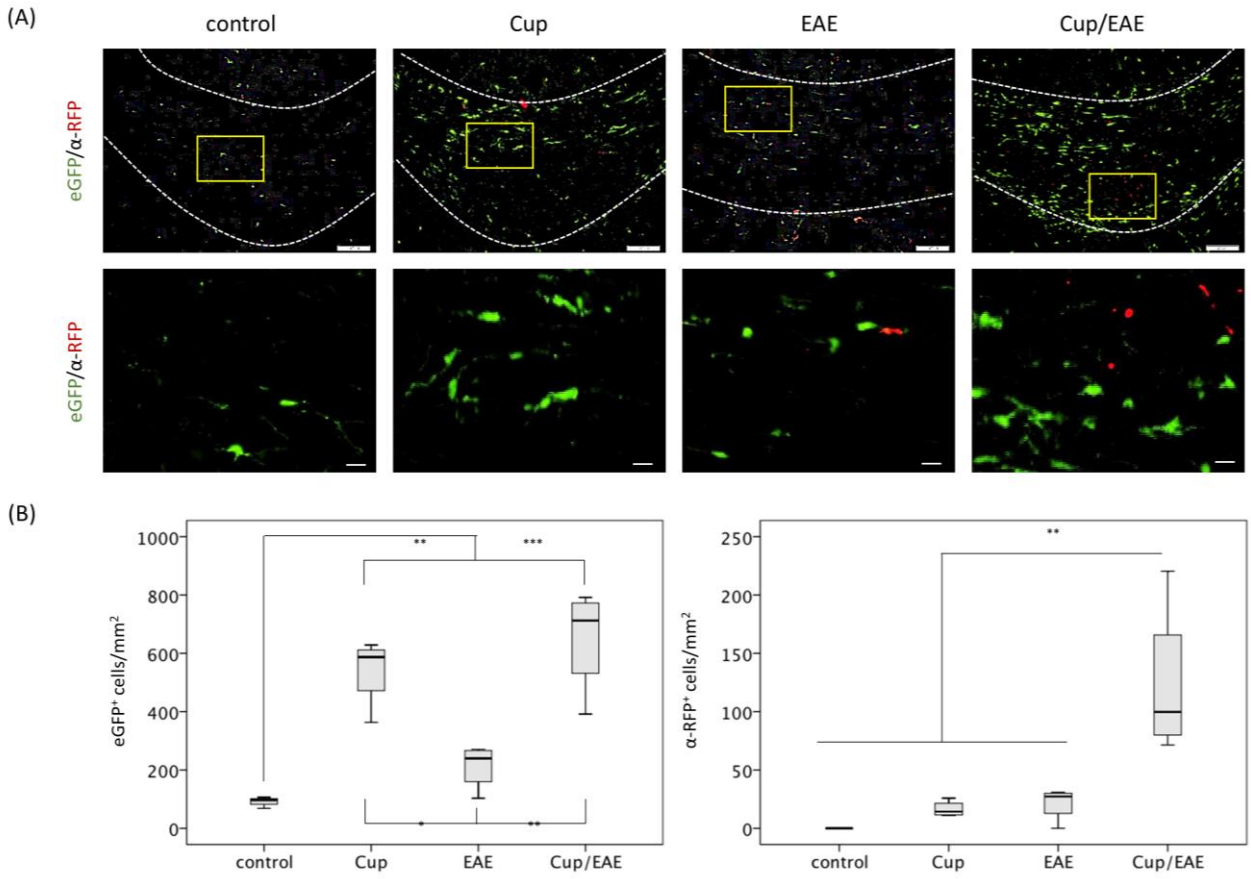

Figure 4. Monocyte recruitment in Cup/EAE mice.

(A) Representative images of the splenia of the corpus callosa (delineated by dotted lines) from control, Cup, EAE, and Cup/EAE mice showing microglia (green) and infiltrating monocytes (red). The Scale bars indicate 100 μm (top) and 10 μm (bottom). (B) Microglia and macrophage densities within the splenia of the corpus callosa from control (n = 3), Cup (n = 4), EAE (n = 4), and Cup/EAE (n = 4) mice; *p < 0.05, **p < 0.01, and ***p < 0.001 via one-way ANOVAs with Tukey's post-hoc tests.

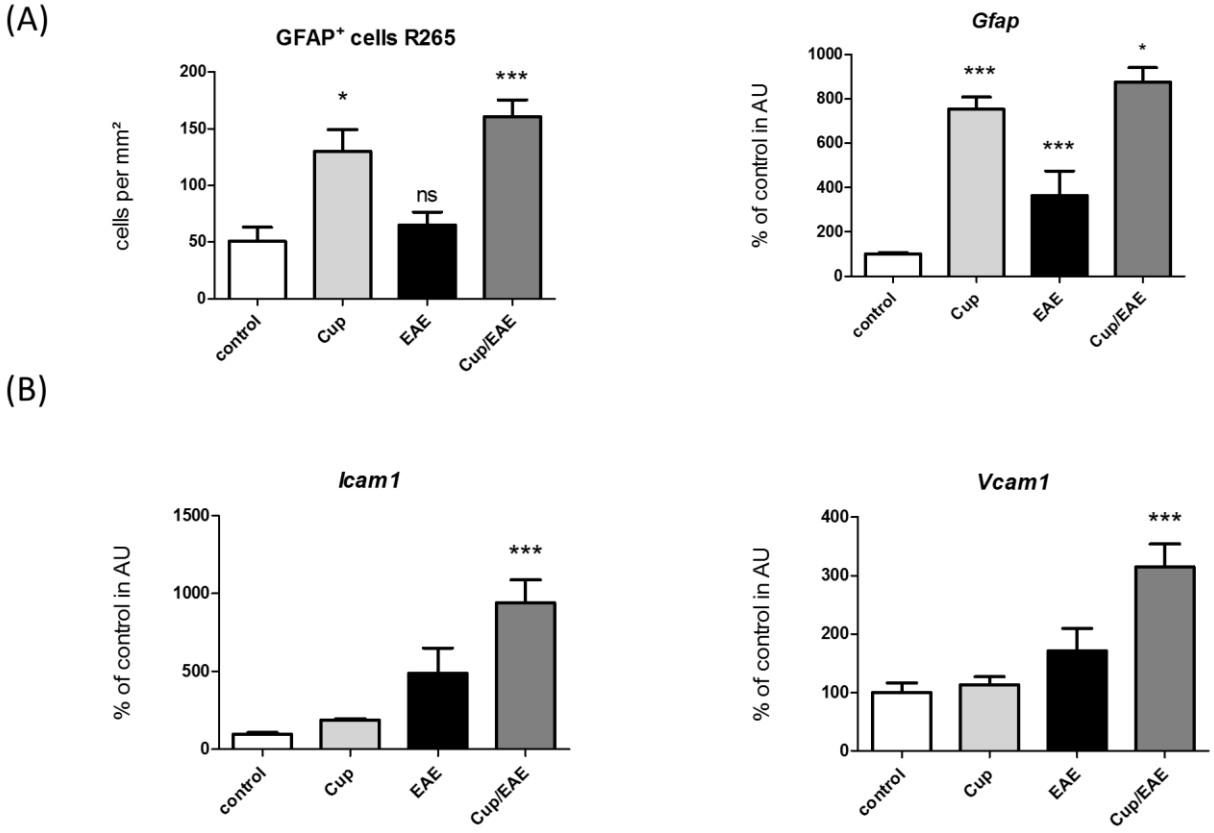

Figure 5. Induction of cell adhesion molecules in Cup/EAE mice.

(A) Quantification of GFAP$^+$ astrocytes and *Gfap* mRNA levels in medial parts of the corpus callosum show similar inductions in Cup and Cup/EAE treatment groups. (B) mRNA expression levels of intercellular adhesion molecule 1 (*Icam1*) and vascular cell adhesion molecule 1 (*Vcam1*) in control (n = 5), Cup (n = 5), EAE (n = 4), and Cup/EAE (n = 5) mice; *p < 0.05 and ***p < 0.001 vs. controls via one-way ANOVAs with Dunnett's post-hoc test. ns, not significant.

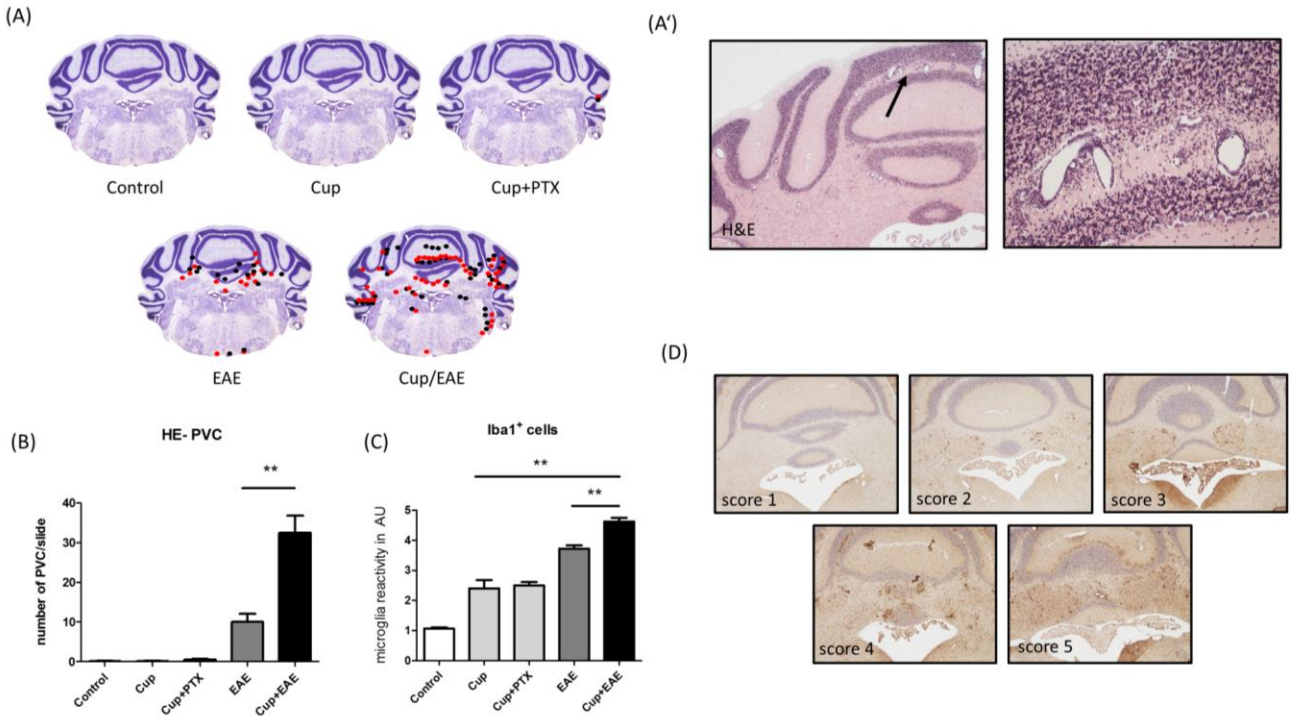

481 **Figure 6. Cerebellar inflammatory cell infiltration.**

482 (A) Spatial distribution of loci of perivascular infiltrates (red and black dots from two independent
483 observers) in cerebella. (A′) Representative images of perivascular infiltrates in the cerebellum (H&E
484 staining). (B) Number of perivascular infiltrates in different treatment groups. (C,D) The extent of
485 microglia/monocyte activation was determined by blinded scoring (1, normal; 5, maximum activity; see
486 panel D for representative images) of Iba1 immunoreactivity; *$p < 0.05$, **$p < 0.01$, and ***$p < 0.001$
487 via Mann Whitney tests.

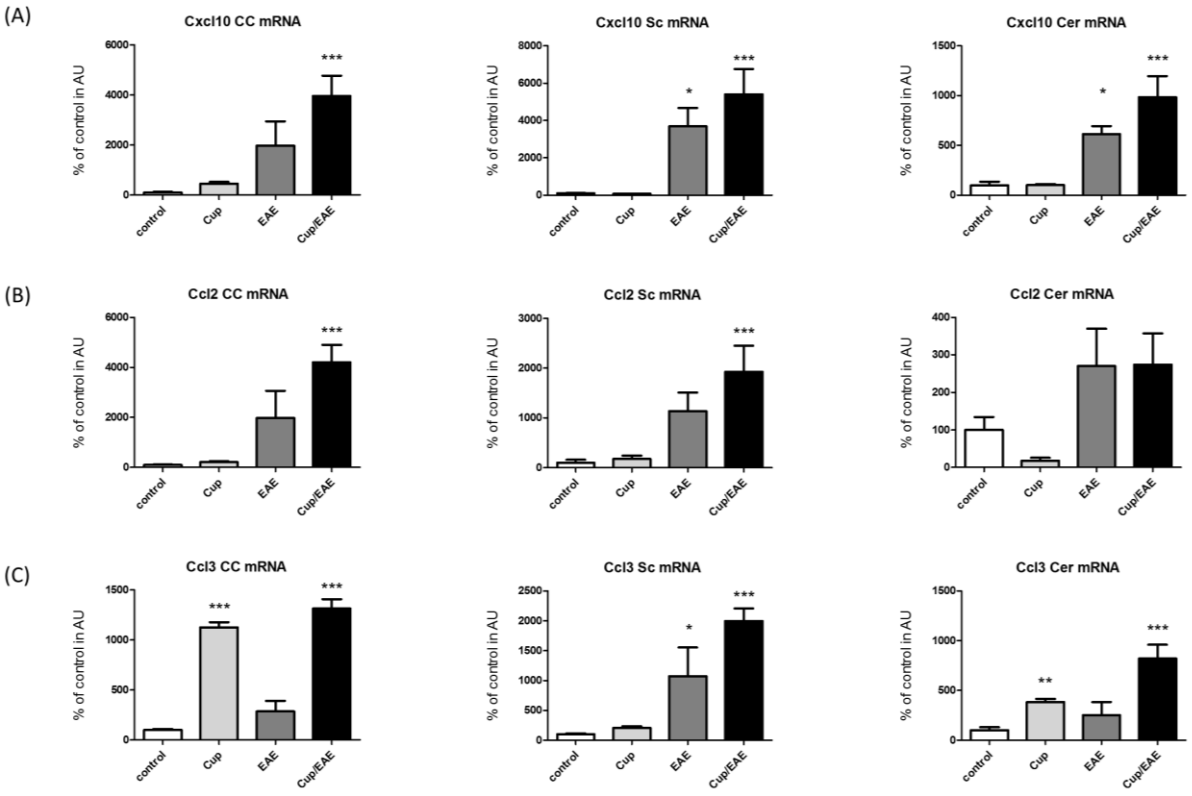

488 **Figure 7. Chemokine expression.**

489 mRNA expression levels of the chemokines C-X-C motif ligand 10 (*Cxcl10*) (A), C-C motif ligand 2
490 (*Ccl2*) (B), and C-C motif ligand 3 (*Ccl3*) (C) in the corpus callosum (CC), spinal cord (Sc) and
491 cerebellum (Cer). Comparisons of the mRNA levels between control (n = 5), Cup (n = 5), EAE (n = 4),
492 and Cup/EAE (n = 5) mice were conducted using one-way ANOVAs with Dunnett's post-hoc tests; *p
493 < 0.05, **p < 0.01, and ***p < 0.001 vs. control.

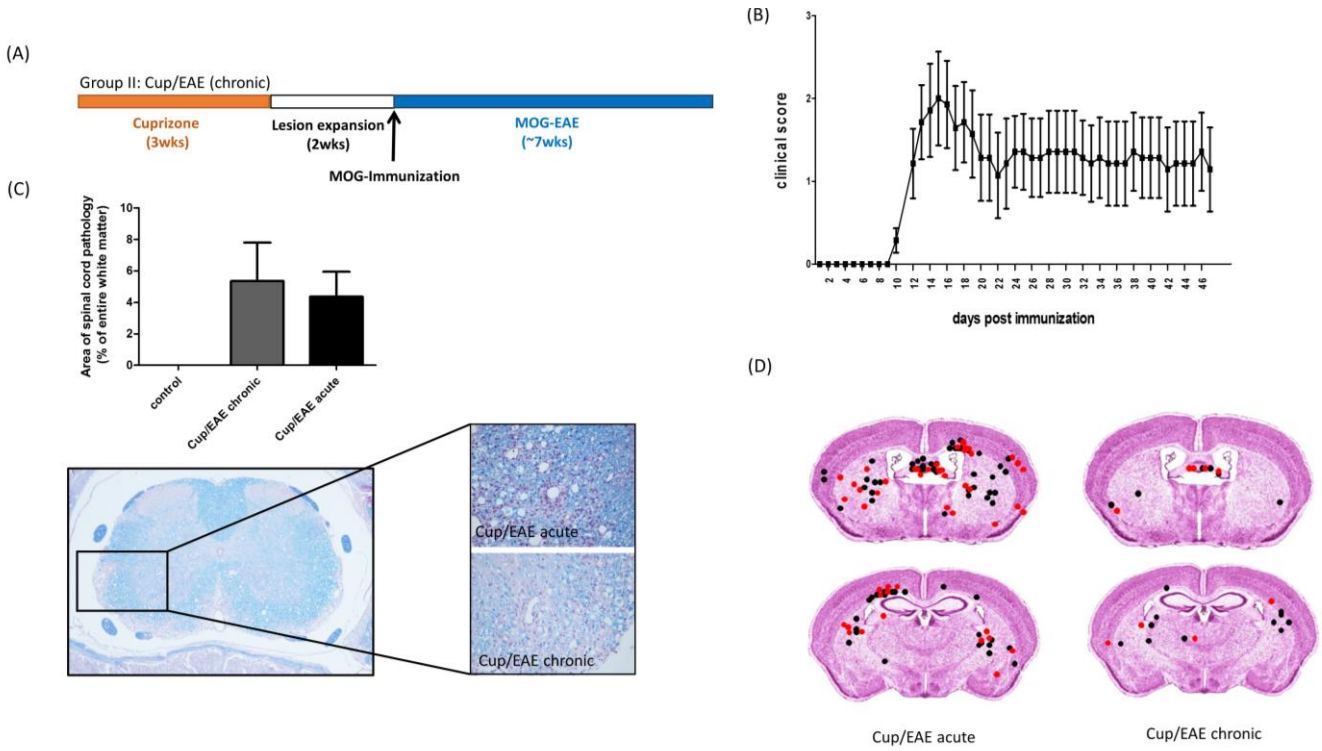

Figure 8. Lesions during the chronic disease stage in Cup/EAE mice.

(A) Schematic depicting the experimental setup. Period of cuprizone intoxication is highlighted in orange, whereas the period for $MOG_{35–55}$ immunization and subsequent active EAE development is highlighted in blue. (B) Clinical scores of Cup/EAE (chronic) mice. (C) Spinal cord pathology in Cup/EAE mice during acute and chronic stages (LFB/periodic acid-Schiff staining). (D) Distribution of perivascular infiltrates in the forebrains of Cup/EAE mice during acute and chronic stages (H&E staining). Analysis was performed by two independent observers (red and black dots).

References

Acs, P., Kipp, M., Norkute, A., Johann, S., Clarner, T., Braun, A., . . . Beyer, C. (2009). 17beta-estradiol and progesterone prevent cuprizone provoked demyelination of corpus callosum in male mice. *Glia, 57*(8), 807-814. doi:10.1002/glia.20806

Alvarez, J. I., Katayama, T., & Prat, A. (2013). Glial influence on the blood brain barrier. *Glia, 61*(12), 1939-1958. doi:10.1002/glia.22575

Aube, B., Levesque, S. A., Pare, A., Chamma, E., Kebir, H., Gorina, R., . . . Lacroix, S. (2014). Neutrophils mediate blood-spinal cord barrier disruption in demyelinating neuroinflammatory diseases. *J Immunol, 193*(5), 2438-2454. doi:10.4049/jimmunol.1400401

Bakker, D. A., & Ludwin, S. K. (1987). Blood-brain barrier permeability during Cuprizone-induced demyelination. Implications for the pathogenesis of immune-mediated demyelinating diseases. *J Neurol Sci, 78*(2), 125-137.

Barnett, M. H., & Prineas, J. W. (2004). Relapsing and remitting multiple sclerosis: pathology of the newly forming lesion. *Ann Neurol, 55*(4), 458-468. doi:10.1002/ana.20016

Bauer, J., Rauschka, H., & Lassmann, H. (2001). Inflammation in the nervous system: the human perspective. *Glia, 36*(2), 235-243.

Baxi, E. G., DeBruin, J., Tosi, D. M., Grishkan, I. V., Smith, M. D., Kirby, L. A., . . . Gocke, A. R. (2015). Transfer of myelin-reactive th17 cells impairs endogenous remyelination in the central nervous system of cuprizone-fed mice. *J Neurosci, 35*(22), 8626-8639. doi:10.1523/jneurosci.3817-14.2015

Benn, T., Halfpenny, C., & Scolding, N. (2001). Glial cells as targets for cytotoxic immune mediators. *Glia, 36*(2), 200-211.

Berghoff, S. A., Gerndt, N., Winchenbach, J., Stumpf, S. K., Hosang, L., Odoardi, F., . . . Saher, G. (2017). Dietary cholesterol promotes repair of demyelinated lesions in the adult brain. *Nat Commun, 8*, 14241. doi:10.1038/ncomms14241

Bitsch, A., Schuchardt, J., Bunkowski, S., Kuhlmann, T., & Bruck, W. (2000). Acute axonal injury in multiple sclerosis. Correlation with demyelination and inflammation. *Brain, 123 (Pt 6)*, 1174-1183.

Boretius, S., Escher, A., Dallenga, T., Wrzos, C., Tammer, R., Bruck, W., . . . Stadelmann, C. (2012). Assessment of lesion pathology in a new animal model of MS by multiparametric MRI and DTI. *Neuroimage, 59*(3), 2678-2688. doi:10.1016/j.neuroimage.2011.08.051

Carlson, T., Kroenke, M., Rao, P., Lane, T. E., & Segal, B. (2008). The Th17-ELR+ CXC chemokine pathway is essential for the development of central nervous system autoimmune disease. *J Exp Med, 205*(4), 811-823. doi:10.1084/jem.20072404

Carr, M. W., Roth, S. J., Luther, E., Rose, S. S., & Springer, T. A. (1994). Monocyte chemoattractant protein 1 acts as a T-lymphocyte chemoattractant. *Proc Natl Acad Sci U S A, 91*(9), 3652-3656.

Charcot, M. (1868). Histologie de la sclerose en plaque. *Gaz. Hosp, 41*, 554-556.

Clarner, T., Diederichs, F., Berger, K., Denecke, B., Gan, L., van der Valk, P., . . . Kipp, M. (2012). Myelin debris regulates inflammatory responses in an experimental demyelination animal model and multiple sclerosis lesions. *Glia, 60*(10), 1468-1480. doi:10.1002/glia.22367

Clarner, T., Janssen, K., Nellessen, L., Stangel, M., Skripuletz, T., Krauspe, B., . . . Kipp, M. (2015). CXCL10 triggers early microglial activation in the cuprizone model. *J Immunol, 194*(7), 3400-3413. doi:10.4049/jimmunol.1401459

Codarri, L., Greter, M., & Becher, B. (2013). Communication between pathogenic T cells and myeloid cells in neuroinflammatory disease. *Trends Immunol, 34*(3), 114-119. doi:10.1016/j.it.2012.09.007

Cua, D. J., Sherlock, J., Chen, Y., Murphy, C. A., Joyce, B., Seymour, B., . . . Sedgwick, J. D. (2003). Interleukin-23 rather than interleukin-12 is the critical cytokine for autoimmune inflammation of the brain. *Nature, 421*(6924), 744-748. doi:10.1038/nature01355

Dooley, D., Lemmens, E., Vangansewinkel, T., Le Blon, D., Hoornaert, C., Ponsaerts, P., & Hendrix, S. (2016). Cell-Based Delivery of Interleukin-13 Directs Alternative Activation of Macrophages

Resulting in Improved Functional Outcome after Spinal Cord Injury. *Stem Cell Reports, 7*(6), 1099-1115. doi:10.1016/j.stemcr.2016.11.005

Gehrmann, J., Banati, R. B., Cuzner, M. L., Kreutzberg, G. W., & Newcombe, J. (1995). Amyloid precursor protein (APP) expression in multiple sclerosis lesions. *Glia, 15*(2), 141-151. doi:10.1002/glia.440150206

Glad, S. B., Nyland, H. I., Aarseth, J. H., Riise, T., & Myhr, K. M. (2009). Long-term follow-up of benign multiple sclerosis in Hordaland County, Western Norway. *Mult Scler, 15*(8), 942-950. doi:10.1177/1352458509106511

Groebe, A., Clarner, T., Baumgartner, W., Dang, J., Beyer, C., & Kipp, M. (2009). Cuprizone treatment induces distinct demyelination, astrocytosis, and microglia cell invasion or proliferation in the mouse cerebellum. *Cerebellum, 8*(3), 163-174. doi:10.1007/s12311-009-0099-3

Hartung, H. P., Aktas, O., Menge, T., & Kieseier, B. C. (2014). Immune regulation of multiple sclerosis. *Handb Clin Neurol, 122*, 3-14. doi:10.1016/b978-0-444-52001-2.00001-7

Hertwig, L., Pache, F., Romero-Suarez, S., Sturner, K. H., Borisow, N., Behrens, J., . . . Paul, F. (2016). Distinct functionality of neutrophils in multiple sclerosis and neuromyelitis optica. *Mult Scler, 22*(2), 160-173. doi:10.1177/1352458515586084

Hiremath, M. M., Chen, V. S., Suzuki, K., Ting, J. P., & Matsushima, G. K. (2008). MHC class II exacerbates demyelination in vivo independently of T cells. *J Neuroimmunol, 203*(1), 23-32. doi:10.1016/j.jneuroim.2008.06.034

Hoflich, K. M., Beyer, C., Clarner, T., Schmitz, C., Nyamoya, S., Kipp, M., & Hochstrasser, T. (2016). Acute axonal damage in three different murine models of multiple sclerosis: A comparative approach. *Brain Res, 1650*, 125-133. doi:10.1016/j.brainres.2016.08.048

Iglesias, A., Bauer, J., Litzenburger, T., Schubart, A., & Linington, C. (2001). T- and B-cell responses to myelin oligodendrocyte glycoprotein in experimental autoimmune encephalomyelitis and multiple sclerosis. *Glia, 36*(2), 220-234.

Iwakura, Y., Ishigame, H., Saijo, S., & Nakae, S. (2011). Functional specialization of interleukin-17 family members. *Immunity, 34*(2), 149-162. doi:10.1016/j.immuni.2011.02.012

Kilic, A. K., Esendagli, G., Sayat, G., Talim, B., Karabudak, R., & Kurne, A. T. (2015). Promotion of experimental autoimmune encephalomyelitis upon neutrophil granulocytes' stimulation with formyl-methionyl-leucyl-phenylalanine (fMLP) peptide. *Autoimmunity, 48*(6), 423-428. doi:10.3109/08916934.2015.1030615

Kondo, A., Nakano, T., & Suzuki, K. (1987). Blood-brain barrier permeability to horseradish peroxidase in twitcher and cuprizone-intoxicated mice. *Brain Res, 425*(1), 186-190.

Korn, T., Reddy, J., Gao, W., Bettelli, E., Awasthi, A., Petersen, T. R., . . . Kuchroo, V. K. (2007). Myelin-specific regulatory T cells accumulate in the CNS but fail to control autoimmune inflammation. *Nat Med, 13*(4), 423-431. doi:10.1038/nm1564

Kornek, B., Storch, M. K., Weissert, R., Wallstroem, E., Stefferl, A., Olsson, T., . . . Lassmann, H. (2000). Multiple sclerosis and chronic autoimmune encephalomyelitis: a comparative quantitative study of axonal injury in active, inactive, and remyelinated lesions. *Am J Pathol, 157*(1), 267-276. doi:10.1016/s0002-9440(10)64537-3

Kuerten, S., Kostova-Bales, D. A., Frenzel, L. P., Tigno, J. T., Tary-Lehmann, M., Angelov, D. N., & Lehmann, P. V. (2007). MP4- and MOG:35-55-induced EAE in C57BL/6 mice differentially targets brain, spinal cord and cerebellum. *J Neuroimmunol, 189*(1-2), 31-40. doi:10.1016/j.jneuroim.2007.06.016

Kuhlmann, T., Lingfeld, G., Bitsch, A., Schuchardt, J., & Bruck, W. (2002). Acute axonal damage in multiple sclerosis is most extensive in early disease stages and decreases over time. *Brain, 125*(Pt 10), 2202-2212.

Le Blon, D., Guglielmetti, C., Hoornaert, C., Quarta, A., Daans, J., Dooley, D., . . . Ponsaerts, P. (2016). Intracerebral transplantation of interleukin 13-producing mesenchymal stem cells limits microgliosis, oligodendrocyte loss and demyelination in the cuprizone mouse model. *J Neuroinflammation, 13*(1), 288. doi:10.1186/s12974-016-0756-7

Liu, K. K., & Dorovini-Zis, K. (2012). Differential regulation of CD4+ T cell adhesion to cerebral microvascular endothelium by the beta-chemokines CCL2 and CCL3. *Int J Mol Sci, 13*(12), 16119-16140. doi:10.3390/ijms131216119

Liu, L., Belkadi, A., Darnall, L., Hu, T., Drescher, C., Cotleur, A. C., . . . Ransohoff, R. M. (2010). CXCR2-positive neutrophils are essential for cuprizone-induced demyelination: relevance to multiple sclerosis. *Nat Neurosci, 13*(3), 319-326. doi:10.1038/nn.2491

Liu, Y., Holdbrooks, A. T., Meares, G. P., Buckley, J. A., Benveniste, E. N., & Qin, H. (2015). Preferential Recruitment of Neutrophils into the Cerebellum and Brainstem Contributes to the Atypical Experimental Autoimmune Encephalomyelitis Phenotype. *J Immunol, 195*(3), 841-852. doi:10.4049/jimmunol.1403063

Lublin, F. D., Reingold, S. C., Cohen, J. A., Cutter, G. R., Sorensen, P. S., Thompson, A. J., . . . Polman, C. H. (2014). Defining the clinical course of multiple sclerosis: the 2013 revisions. *Neurology, 83*(3), 278-286. doi:10.1212/wnl.0000000000000560

Lucchinetti, C., Bruck, W., Parisi, J., Scheithauer, B., Rodriguez, M., & Lassmann, H. (2000). Heterogeneity of multiple sclerosis lesions: implications for the pathogenesis of demyelination. *Ann Neurol, 47*(6), 707-717.

McGeachy, M. J., Stephens, L. A., & Anderton, S. M. (2005). Natural recovery and protection from autoimmune encephalomyelitis: contribution of CD4+CD25+ regulatory cells within the central nervous system. *J Immunol, 175*(5), 3025-3032.

McMahon, E. J., Suzuki, K., & Matsushima, G. K. (2002). Peripheral macrophage recruitment in cuprizone-induced CNS demyelination despite an intact blood-brain barrier. *J Neuroimmunol, 130*(1-2), 32-45.

Mildner, A., Schmidt, H., Nitsche, M., Merkler, D., Hanisch, U. K., Mack, M., . . . Prinz, M. (2007). Microglia in the adult brain arise from Ly-6ChiCCR2+ monocytes only under defined host conditions. *Nat Neurosci, 10*(12), 1544-1553. doi:10.1038/nn2015

Millward, J. M., Caruso, M., Campbell, I. L., Gauldie, J., & Owens, T. (2007). IFN-gamma-induced chemokines synergize with pertussis toxin to promote T cell entry to the central nervous system. *J Immunol, 178*(12), 8175-8182.

Moreno, M., Bannerman, P., Ma, J., Guo, F., Miers, L., Soulika, A. M., & Pleasure, D. (2014). Conditional ablation of astroglial CCL2 suppresses CNS accumulation of M1 macrophages and preserves axons in mice with MOG peptide EAE. *J Neurosci, 34*(24), 8175-8185. doi:10.1523/jneurosci.1137-14.2014

Noell, S., Wolburg-Buchholz, K., Mack, A. F., Ritz, R., Tatagiba, M., Beschorner, R., . . . Fallier-Becker, P. (2012). Dynamics of expression patterns of AQP4, dystroglycan, agrin and matrix metalloproteinases in human glioblastoma. *Cell Tissue Res, 347*(2), 429-441. doi:10.1007/s00441-011-1321-4

Norkute, A., Hieble, A., Braun, A., Johann, S., Clarner, T., Baumgartner, W., . . . Kipp, M. (2009). Cuprizone treatment induces demyelination and astrocytosis in the mouse hippocampus. *J Neurosci Res, 87*(6), 1343-1355. doi:10.1002/jnr.21946

Nunes, J. C., Radbruch, H., Walz, R., Lin, K., Stenzel, W., Prokop, S., . . . Heppner, F. L. (2015). The most fulminant course of the Marburg variant of multiple sclerosis-autopsy findings. *Mult Scler, 21*(4), 485-487. doi:10.1177/1352458514537366

Park, H., Li, Z., Yang, X. O., Chang, S. H., Nurieva, R., Wang, Y. H., . . . Dong, C. (2005). A distinct lineage of CD4 T cells regulates tissue inflammation by producing interleukin 17. *Nat Immunol, 6*(11), 1133-1141. doi:10.1038/ni1261

Pfeifenbring, S., Bunyan, R. F., Metz, I., Rover, C., Huppke, P., Gartner, J., . . . Bruck, W. (2015). Extensive acute axonal damage in pediatric multiple sclerosis lesions. *Ann Neurol, 77*(4), 655-667. doi:10.1002/ana.24364

Pierson, E. R., Wagner, C. A., & Goverman, J. M. (2016). The contribution of neutrophils to CNS autoimmunity. *Clin Immunol*. doi:10.1016/j.clim.2016.06.017

Price, P. J., Luckow, B., Torres-Dominguez, L. E., Brandmuller, C., Zorn, J., Kirschning, C. J., . . . Lehmann, M. H. (2014). Chemokine (C-C Motif) receptor 1 is required for efficient

recruitment of neutrophils during respiratory infection with modified vaccinia virus Ankara. *J Virol, 88*(18), 10840-10850. doi:10.1128/jvi.01524-14

Rush, C. A., MacLean, H. J., & Freedman, M. S. (2015). Aggressive multiple sclerosis: proposed definition and treatment algorithm. *Nat Rev Neurol, 11*(7), 379-389. doi:10.1038/nrneurol.2015.85

Saederup, N., Cardona, A. E., Croft, K., Mizutani, M., Cotleur, A. C., Tsou, C. L., . . . Charo, I. F. (2010). Selective chemokine receptor usage by central nervous system myeloid cells in CCR2-red fluorescent protein knock-in mice. *PLoS One, 5*(10), e13693. doi:10.1371/journal.pone.0013693

Sartori, A., Abdoli, M., & Freedman, M. S. (2017). Can we predict benign multiple sclerosis? Results of a 20-year long-term follow-up study. *J Neurol, 264*(6), 1068-1075. doi:10.1007/s00415-017-8487-y

Scheld, M., Ruther, B. J., Grosse-Veldmann, R., Ohl, K., Tenbrock, K., Dreymuller, D., . . . Kipp, M. (2016). Neurodegeneration Triggers Peripheral Immune Cell Recruitment into the Forebrain. *J Neurosci, 36*(4), 1410-1415. doi:10.1523/jneurosci.2456-15.2016

Schirmer, L., Merkler, D., Konig, F. B., Bruck, W., & Stadelmann, C. (2013). Neuroaxonal regeneration is more pronounced in early multiple sclerosis than in traumatic brain injury lesions. *Brain Pathol, 23*(1), 2-12. doi:10.1111/j.1750-3639.2012.00608.x

Serada, S., Fujimoto, M., Mihara, M., Koike, N., Ohsugi, Y., Nomura, S., . . . Naka, T. (2008). IL-6 blockade inhibits the induction of myelin antigen-specific Th17 cells and Th1 cells in experimental autoimmune encephalomyelitis. *Proceedings of the National Academy of Sciences of the United States of America, 105*(26), 9041-9046. doi:10.1073/pnas.0802218105

Skripuletz, T., Bussmann, J. H., Gudi, V., Koutsoudaki, P. N., Pul, R., Moharregh-Khiabani, D., . . . Stangel, M. (2010). Cerebellar cortical demyelination in the murine cuprizone model. *Brain Pathol, 20*(2), 301-312. doi:10.1111/j.1750-3639.2009.00271.x

Slowik, A., Schmidt, T., Beyer, C., Amor, S., Clarner, T., & Kipp, M. (2015). The sphingosine 1-phosphate receptor agonist FTY720 is neuroprotective after cuprizone-induced CNS demyelination. *Br J Pharmacol, 172*(1), 80-92. doi:10.1111/bph.12938

Steinbach, K., Piedavent, M., Bauer, S., Neumann, J. T., & Friese, M. A. (2013). Neutrophils amplify autoimmune central nervous system infiltrates by maturing local APCs. *J Immunol, 191*(9), 4531-4539. doi:10.4049/jimmunol.1202613

Trapp, B. D., Ransohoff, R., & Rudick, R. (1999). Axonal pathology in multiple sclerosis: relationship to neurologic disability. *Curr Opin Neurol, 12*(3), 295-302.

Werner, K., Bitsch, A., Bunkowski, S., Hemmerlein, B., & Bruck, W. (2002). The relative number of macrophages/microglia expressing macrophage colony-stimulating factor and its receptor decreases in multiple sclerosis lesions. *Glia, 40*(1), 121-129. doi:10.1002/glia.10120

Wu, F., Cao, W., Yang, Y., & Liu, A. (2010). Extensive infiltration of neutrophils in the acute phase of experimental autoimmune encephalomyelitis in C57BL/6 mice. *Histochem Cell Biol, 133*(3), 313-322. doi:10.1007/s00418-009-0673-2

Xu, L. L., Warren, M. K., Rose, W. L., Gong, W., & Wang, J. M. (1996). Human recombinant monocyte chemotactic protein and other C-C chemokines bind and induce directional migration of dendritic cells in vitro. *J Leukoc Biol, 60*(3), 365-371.

Zimmermann, J., Emrich, M., Krauthausen, M., Saxe, S., Nitsch, L., Heneka, M. T., . . . Muller, M. (2017). IL-17A Promotes Granulocyte Infiltration, Myelin Loss, Microglia Activation, and Behavioral Deficits During Cuprizone-Induced Demyelination. *Mol Neurobiol*. doi:10.1007/s12035-016-0368-3